Overcoming Small-Bandgap Charge Recombination in Visible and NIR-Light-Driven Hydrogen Evolution by Engineering the Polymer Photocatalyst Structure

Mohamed Elsayed
National Tsing Hua University
Mohamed Abdelah
Uppsala University
Islam Mekhemer
National Tsing Hua University
Ahmed Aboubakr
Academia Sinica
Mohamed Mohamed
National Sun Yat-Sen University
Shiao-Wei Kuo
National Sun Yat-Sen University https://orcid.org/0000-0002-4306-7171
Chen-Hsiung Hung
Academia Sinica
Li-Chyong Chen
National Taiwan University https://orcid.org/0000-0001-6373-7729
Kuei-Hsien Chen
Institute of Atomic and Molecular Sciences, Academia Sinica https://orcid.org/0000-0002-9397-2516
Ho-Hsiu Chou (hhchou@mx.nthu.edu.tw)
Departments of Chemical Engineering, National Tsing Hua University https://orcid.org/0000-0003-3777-2277

Article

Keywords: π-linker effect, near-infrared photocatalyst, polymer dots photocatalysts, visible-light, hydrogen evolution, ITIC-polymers

Posted Date: January 4th, 2023

DOI: https://doi.org/10.21203/rs.3.rs-2322142/v1

Abstract

Designing an organic polymer photocatalyst for efficient hydrogen evolution with visible and near-infrared (NIR) light activity is still a major challenge. Unlike the common behaviour of increasing the charge recombination gradually while shrinking the bandgap, here we present a series of polymers nanoparticles (Pdots) based on ITIC and BTIC units with different π-linkers between the acceptor-donor-acceptor (A-D-A) repeated moieties of the polymer, which acts as an efficient single polymer photocatalyst for H_2 evolution under both visible and NIR light without combining or hybridizing with other materials. Importantly, the difluorothiophene (ThF) π-linker facilitates the charge transfer between acceptors of different repeated moieties (~ A-D-A-(π-Linker)-A-D-A~) leading to enhancement of charge separation between D and A. As a result, the PITIC-ThF Pdots exhibit superior hydrogen evolution rates of 339.7 mmol g^{-1} h^{-1} (0.279 mol/h) and 4100 μmol g^{-1} h^{-1} (20.5 μmol/h) with visible (> 420 nm) and NIR (> 780 nm) light irradiation, respectively. Furthermore, PITIC-ThF Pdots exhibit a record-breaking apparent quantum yield (AQY) at 700 nm (4.76%).

Introduction

Organic photocatalysts have attracted attention as a new photocatalyst approach due to their tuneable bandgap and notable ability to modify the molecular structure.[1, 2, 3, 4, 5] However, the hydrophobic nature of the majority of conjugated polymers counts as a problem that minimizes their water dispersity [6, 7, 8] so some amphiphilic surfactants utilized to convert the pulk polymer to polymer nanoparticles (Pdot) which enhanced their water dispersity, increase the active area and reduce the diffusion length of the charge carrier.[9, 10, 11, 12] Many series of conjugated polymers have been reported as photocatalysts for hydrogen production under UV and visible light irradiation without including the near-infrared (NIR) region, which represents more than 50% of the solar radiation spectrum.[13, 14, 15, 16, 17, 18, 19] Full harvesting of solar light (from the visible to NIR region) is always the goal and a major challenge for photocatalysts, particularly for the new approach of conjugated polymer photocatalysts because of the insufficient photocatalytic activity of narrow bandgap semiconductors, the direct conversion of NIR light energy into heat, or the low photon energy of NIR light.[20] Unfortunately, only a few photocatalysts reveal NIR activity for H_2 evolution and are mostly limited to composite, heterostructured, or hybridized materials.[21, 22, 23, 24, 25] Regarding organic polymer photocatalysts, there is no prior study presenting a polymer photocatalyst with NIR activity for H_2 evolution. Small molecules of organic semiconductors, named ITIC and BTIC[26, 27], have been widely used for organic solar cell applications because of their narrow bandgap, significant advances due to their efficient light absorption in the visible and NIR regions, high charge mobility, and easily tuned energy level[28, 29, 30]. The ITIC structure consists of a bulky fused aromatic ring as a core donor (D) with two terminal acceptors (A) of 1,1-dicyanomethylene-3-indanone, which is constructed as A-D-A, and ITIC stands for 2,2'-[[6,6,12,12-tetrakis(4-hexylphenyl)-6,12-dihydrodithieno[2,3-d:2',3-d']-s-indaceno[1,2-b:5,6-b']dithiophene-2,8-diyl]-bis[methylidyne(3-oxo-1*H*-indene-2,1(3*H*)-diylidene)]]bis(propanedinitrile)).[31] BTIC is constructed as A-DAD-A and stands for (2,2'-((2Z,2'Z)-((12,13-

bis(2-ethylhexyl)-3,9-diundecyl-12,13-dihydro-[1, 2, 5]thiadiazolo[3,4-e]thieno[2",3":4',5'] thieno [2',3':4,5] pyrrolo [3,2g] thieno [2',3':4,5] thieno [3,2-b] indole-2,10-diyl) bis(methanylidene)) bis(3-oxo-2,3-dihydro-1*H*-indene-2,1-diylidene))dimalononitrile).[32] Very recently, Tian's group, Cooper's group, and McCulloch group integrated ITIC or BTIC small molecules as acceptors with other donor polymers to construct a hybrid photocatalyst for hydrogen evolution.[7, 9, 33] The notable ability to modify the molecular structure of organic materials allows us to construct a series of ITIC- and BTIC-based polymers that can absorb a broad range of the solar spectrum, including the visible and NIR regions with avoiding the charge recombination simultaneously.

Here, we demonstrated a series of ITIC- and BTIC-based polymeric photocatalysts for H_2 evolution under visible and NIR light without combining or hybridizing with other materials. Our molecular design is based on introducing and tuning the π-linker between ITIC or BTIC repeated moiety of the polymer to get polymer structure of ~ A-D-A-(π-linker)-A-D-A ~ and ~ A-DA$D-A-(\pi-l\in ker)-A-DA$D-A~, respectively (Fig. 1). Three different π-linkers (X), namely, phenyl (Ph), thiophene (Th), and 3,4-difluorothiophene (ThF) units are used as comonomers on the terminal acceptor ring at the C-5 and C-6 positions for polymerization by cross coupling methods (Fig. 1). The use of different π-linker groups results in structures with different planarity, which affects the conjugation and charge transfer between acceptors of different repeated moieties of the polymer, and leads to flexibility in terms of tuning the bandgap and absorption properties of polymers as well as the charge separation between D and A during the photocatalytic reaction. Interestingly, unlike the common behaviour of increasing the charge recombination gradually while shrinking the bandgap, our constructed polymer with ThF π-linker can redshift the absorption to the NIR region and enhance the charge separation between D and A simultaneously (Fig. 1). Moreover, the higher crystallinity of PITIC-based polymer, as well as the charge distribution between A and A` of the PBTIC-based polymer, explain the superiority of the first over the second in regard to photocatalytic activity. In the end, the demonstrated polymers are converted from bulk to Pdots to overcome the water dispersity issue of hydrophobic polymers and prevent the use of eco-solvents during the photocatalytic reaction. Studying the effect of different surfactants allows us to prepare MeOH and surfactant-free Pdots as promising photocatalysts for hydrogen production from water.

Result And Discussion

Polymer and Pdots preparation and characterizations

The synthesis routes of the designed new series of PITIC-X-[34] and PBTIC-X-based conjugated polymers are shown in **Schemes S1 – S4**. Accordingly, we synthesized the three PITIC-X and PBTIC-X-based polymers through Suzuki Miyaura and Stille coupling polymerizations, resulting in the polymers PITIC-Ph, PITIC-Th, PITIC-ThF, PBTIC-Ph, PBTIC-Th, and PBTIC-ThF respectively, and the detailed procedures are described in the Supporting Information. The as-prepared polymers were characterized by ^{1}H nuclear magnetic resonance (NMR) spectroscopy (**Figures S1 – S10**), thermogravimetric analysis (TGA) (**Table S1**

and Figure S11), Fourier transform infrared (FTIR) spectroscopy (**Figure S12a**), and X-ray photoelectron spectroscopy (XPS) **(Figure S12b, S13, S14, and S15)**.

The bulk polymer was converted to polymer nanoparticles (Pdots) using precipitation methods by dispersing the polymer in water without additional surfactants, such as PS-PEG-COOH or Triton under vigorous sonication, and the preparation details are shown in the Supplementary Information (**Figure S16**). The photographs of all six polymers show different colors in THF solutions, suggesting that their optical properties are easily tuned by the introduction of π-linker units on acceptor rings (Figs. 2a**)**. The normalized ultraviolet–visible (UV–vis) absorption spectra of the six Pdots in water solution are presented in Figs. 2b and the related data are summarized in **Table S2**. The monomer Br-ITIC-Br shows strong absorption in the visible range of 550–750 nm, with λ_{max} at 669 nm and a small shoulder at 620 nm (**Figure S17a)**. The ITIC polymer prepared using the thiophene π-linker (PITIC-Th) exhibits approximately the same absorption onset of Br-ITIC-Br with a slightly blueshifted λ_{max} (657nm). Notably, the substitution of the thiophene group with the phenyl group (PITIC-Ph) is accompanied by a large blueshift leading to λ_{max} of 551 nm. In contrast to the difluorothiophene group (PITIC-ThF), which shows a small new shoulder at 739 nm accompanied by a redshifted absorption onset. This result demonstrates that the introduction of the difluorothiophene group can extend the absorption to the NIR region, which is beneficial for absorbing a large region of the solar spectrum. The as-prepared various comonomer π-linker units with PBTIC-X-based polymers show a redshifted absorption compared to that of PITIC-X-based polymers. This result suggests that the A-DAD-A structure presents larger conjugation than A-D-A, leading to a more highly redshifted absorption (Fig. 2b**)**. Notably, the conversion of the bulk polymers (in THF) to Pdots (in water) is accompanied by a 20 − 50 nm redshift owing to the J aggregation of the polymer chain in aqueous solution,[35, 36] as shown in **Figures S18a and S18b**. According to Tauc plots as shown in **Figures S18c and S18d**, the E_g values of these polymers are in the range of 1.45 − 2.05 eV and become lower in water solutions by approximately 0.10 eV, thereby exhibiting their narrow bandgap that facilitates absorption over a broad range of visible and NIR light. As shown in Fig. 2c, the various π-linker groups have an obvious influence on the energy level positions of the PITIC- and PBTIC-based polymers. The constructed polymers achieve deeper HOMO and LUMO values with the following arrangement of π-linkers ThF > Th > Ph. The previously discussed results indicate that the introduction of different π-linker units on acceptor rings displays a significant effect on the photophysical properties of polymers.

The prepared structure and morphology of the Pdots were determined by cryo-transmission electron microscopy (Cryo-TEM), as shown in Fig. 2d. The six polymers display spherical particles with nonuniform particle sizes ranging from 30 to 70 nm, similar to other reported.[37, 38] The presence of nanometric spherical particles indicates the formation of a Pdot structure from all the polymers. In addition, the sessile drop technique was used to measure the static contact angles of the as-prepared Pdots at three different locations with water at room temperature. The water contact angles of the PITIC-X polymers are lower than those of the PBTIC-X polymers (**Table S2** and **Figure S20**), suggesting that they possess a lower hydrophobicity. Although the as-prepared polymers are hydrophobic, their conversion to the Pdot structure enhances their water dispersion and increases the surface area of the photocatalyst.

Thus, the conversion of hydrophobic polymers to Pdots without the use of any surfactants could be beneficial for achieving good water dispersibility and enhanced hydrogen production from water.

Photocatalytic Activity Under Visible And Nir Light

Next, we examined all the Pdots as photocatalysts for visible light-driven hydrogen evolution. A PAR30 light-emitting diode (LED) lamp (20 W, 6500 K, and λ > 420 nm) was used as the light source (**Figure S21**). The Pt cocatalyst (H_2PtCl_6) with optimized amount of 3% was utilized to enhance the photocatalytic activity of our constructed photocatalysts (**Figure S22**). Under the optimum conditions and visible light illumination, we recorded the kinetic curve of hydrogen evolution to investigate the H_2 evolution efficiency of the photocatalyst, as shown in Fig. 3a. From the kinetic curves, we extracted the H_2 evolution rate of the six polymers (Fig. 3b**)**. Among them, the PITIC-ThF Pdots show the highest HER value (339.7 mmol g^{-1} h^{-1}) followed by the PITIC-Th Pdots (168.7 mmol g^{-1} h^{-1}) and PITIC-Ph Pdots (106.2 mmol g^{-1} h^{-1}). Similar trends are observed for the PBTIC-X series, and the order of the HER is PBTIC-ThF Pdots (269.4 mmol g^{-1} h^{-1}) > PBTIC-Th Pdots (121.1 mmol g^{-1} h^{-1}) > PBTIC-Ph Pdots (69.8 mmol g^{-1} h^{-1}). The HER value increases with increasing photocatalyst amount, in which a loading of 0.1 mg to 5 mg can increase the HER from 34 to 279 μmol/h and 27 to 178 μmol/h for the PITIC-ThF Pdots and PBTIC-ThF Pdots, respectively (Fig. 3c**)**. This result is strong evidence to prove that the high photocatalytic activity of our materials is truly beneficial for the development of hydrogen production under visible light. The photocatalytic activity of the PITIC-ThF Pdots and PBTIC-ThF Pdots under NIR light was investigated using a Xenon lamp (AM1.5 and 3000 W m^{-2}) with a cutoff filter (λ > 780 nm) as a source of light. The amount of H_2 generated from the PITIC-ThF Pdots and PBTIC-ThF Pdots increase over time and reach 11450 ± 800 and 1715 ± 320 μmol/g under NIR light irradiation for 4 h, respectively (Fig. 3d). Among the two polymers with the ThF π-linker, the PITIC-ThF Pdots present an HER of 4045 ± 430 $\mu molh^{-1}g^{-1}$, which is approximately more than 5-fold that of the PBTIC-ThF Pdots (708 ± 210 $\mu molh^{-1}g^{-1}$) (Fig. 3e). The HER of PITIC-ThF Pdot has shown a promising and unprecedented efficiency of a single polymer under NIR light. The apparent quantum yields (AQYs) of the most efficient PITIC-ThF and PBTIC-ThF Pdots were obtained under standard photocatalytic conditions using a light source with a bandpass filter (λ = 420, 500, 550, 600, and 700 nm). As shown in Fig. 3d, the AQYs of the PITIC-ThF (PBTIC-ThF) Pdots are estimated to be 3.9 (2.9), 3.2 (2.7), 3.1 (2.5), 3.9 (2.8), and 4.7% (3.1%) at 420, 500, 550, 600, and 700 nm, respectively. The AQY values are almost compatible with the absorption spectrum of the polymer photocatalyst, with a higher value at a longer wavelength of 700 nm, suggesting that these Pdots have good photoresponsivity for hydrogen production in the entire visible light region. Notably, the HER under visible and NIR light and AQY values at 700 nm of the PITIC-ThF Pdots are among the highest values ever reported in the literature (Fig. 3g, 3h, **and Table S3**). Although some of the reports show a high AQY at 420 nm, it later dramatically decreases when compared to irradiation with a longer wavelength of 700 nm.

Unveiling The Effect Of A-d-a Structure And Different Linkers On The Activity

We explored two important aspects to learn more about the relationship between the structure and activity of the PITIC-X- and PBTIC-X-based polymer photocatalysts: the influence of various π-linkers on polymer activity and the difference between the ITIC and BTIC moieties. The relationship between the different π-linkers and the photocatalytic activity was understood through density functional theory (DFT) and transient absorption (TA) spectroscopy. As shown in **Figures S23 and S24**, the HOMOs of the six polymers are delocalized to some extent over the conjugated systems, whereas the LUMOs are more localized over the IC moiety. Although the different π-linkers does not exhibit a variation in regard to the HOMO and LUMO localization on the main polymer units, the dihedral angles are variable between the different π-linker groups and the IC acceptor moieties. Figure 4a shows that the dihedral angles between the Ph π-linker and IC moiety of PITIC-Ph (34.28°) or PBTIC-Ph (34.34°) are much greater than those between the Th π-linker group and IC moiety of PITIC-Th (23.72°) or PBTIC-Th (23.47°) and those between the ThF π-linker group and IC moiety of PITIC-ThF (18.4°) or PBTIC-ThF (17.66°). This is due to the hydrogen bond formation, namely, H − F and H − S, with the ThF π-linker and only H − S for the Th π-linker, while the Ph π-linker does not show any hydrogen bond formation (**Figure S25**).[39, 40, 41] As a result, the F − H and S − H distances for the ThF π-linker are smaller than the H − H and S − H distances of the Th π-linker, leading to a decrease in the dihedral angles when using the ThF π-linker (**Figure S25**). The smaller dihedral angle between the acceptor and π-linker in PITIC-ThF indicates a more planarized structure with efficient charge carrier mobility and transfer between the acceptors of different repeated moieties followed by improvement of the charge separation between the D and A for every polymer repeated moiety; thus, an enhanced exciton dissociation yield and improved photocatalytic activity are observed. Increasing the dihedral angle with Th and Ph π-linkers reduces the planarity and charge transfer between the acceptors and increase the charge recombination from D to A, resulting in less efficient photocatalytic activity (Fig. 4b). Furthermore, in **Figure S26** the DFT calculations indicating that hydrogen has more affinity to adsorb and that the photocatalytic reaction occurs on the IC acceptor moiety, and compared to the Ph and Th linkers the presence of a ThF in the polymeric structure leads to stronger hydrogen adsorption, which in turn results in more favorable H_2 formation energetics.

Femtosecond transient absorption spectroscopy (fs-TAS) was used to further study the excited state dynamics of the PITIC-X polymers and the effect of the different π-linkers on the excited state lifetime. Figure 5a, 5b, and 5c show the transient absorption spectra of the PITIC-ThF, PITIC-Ph, and PITIC-Th Pdots, respectively. The TA spectra of the three polymers consist of a negative signal assigned to the ground-state bleach of the polymer, which is consistent with the ground-state absorption band, and excited state absorption, which is assigned to the absorption of the polymer excitonic state.[8, 42] Figs. 5d, 5e, and 5f show the bleach recovery dynamics and lifetimes of the three polymers at 564 nm (PITIC-Ph), 650 nm (PITIC-Th), and 650 nm (PITIC-ThF), respectively, which consist of two time components. The results show that the PITIC polymer with different π-linkers shows different bleach recovery dynamics and different lifetimes, where the recombination of photogenerated charge carriers decelerates more in

the following order: ThF > Th > Ph. This is due to the smooth and fast charge transfer between the acceptors of different repeated units in the case of the ThF π-linker with a lower dihedral angle. Moreover, compared to the Th and Ph linkers, the ThF linker with both PITIC and PBTIC polymer series shows strong quenching emission with the steady-state photoluminescence spectra, highest photocurrent responses with the transient photocurrent response, smallest arc radii with the electrochemical impedance spectroscopy (EIS) Nyquist plots (**Figure S27**).

In Fig. 5g, we schematically show the relationship between the different π-linkers and photocatalytic activity according to the previous results. In the case of the Ph π-linker, after photoexcitation, the electrons transfer from D to A, but the large dihedral angle of the Ph π-linker reduces the excited electrons transfer between the acceptors of different repeated moieties, leading to the recombination of photogenerated electrons from A to D, which results in a shorter bleach recovery lifetime and ineffective charge separation. The dihedral angle decreases slightly with the Th π-linker; hence, the transfer of excited electrons between acceptors is enhanced, leading to a relatively long bleach recovery lifetime accompanied by the inhibition of charge recombination and enhancement of charge separation. On the one hand, the ThF π-linker shows effective charge separation and largely decreased charge recombination. This is due to the small dihedral angle presented by the ThF π-linker, which enhances the charge transfer between acceptors of different repeated moieties. In comparison to the PBTIC-X polymers, the PITIC-X polymers have higher photocatalytic activity in the visible and NIR regions. Despite the fact that the PBTIC-ThF absorption spectra redshifts compared to that of PITIC-ThF, the greater effective photocatalytic activity of PITIC-ThF compared to PBTIC-ThF under visible and NIR light is due to the higher crystallinity of PITIC-ThF as well as the charge distribution between A and A` of the PBTIC-based polymer **(Figure S28)**.

Effect Of The Free-surfactant Pdot Structure On The Activity

To clarify the benefits of our presented method for preparing the Pdot structure without additional surfactants, we studied the effect of common surfactants used for Pdot preparation on the photocatalytic activity of the Pdot photocatalyst. The Pdot structure of PITIC-ThF prepared by the precipitation method in the absence and presence of common surfactants, such as PS-PEG-COOH and Triton, produces three Pdot structures: PITIC-ThF Pdots, PITIC-ThF/PS-PEG-COOH Pdots, and PITIC-ThF/Triton Pdots. Compared to the PITIC-ThF Pdots, the PITIC-ThF/PS-PEG-COOH Pdots (Fig. 6a) and PITIC-ThF/Triton Pdots (**Figure S29a**) inhibits the HER. This is due to the resistance arising from the surfactant that can hinder the charge mobility between polymer molecules and charge transfer between the polymer and Pt cocatalyst. Increasing the charge resistance in the presence of surfactants is confirmed by the EIS Nyquist plots, where the arc radius of the PITIC-ThF Pdots is smaller than that of the PS-PEG-COOH/PITIC-ThF Pdots (Fig. 6c), or Triton/PITIC-ThF Pdots (**Figure S29b**). Moreover, the transient absorption traces of the PITIC-ThF Pdots with Pt show a prominent difference in the bleach recovery dynamics and lifetime in the presence and absence of the PS-PEG-COOH surfactant, as shown in Fig. 6b. The presence of PS-PEG-COOH reduces the lifetime from 544 ± 33 ps to 126 ± 36 ps, explaining why the

surfactant can hinder the charge transfer between the polymer and reactant (including the Pt cocatalyst and AA) and then accelerate charge recombination. Figure 6d shows a schematic diagram of the charge transfer from the PITIC-ThF Pdots to the Pt cocatalyst and AA. In the absence of PS-PEG-COOH, the excited electrons transfer to the Pt cocatalyst accompanied by a long bleach recovery lifetime with efficient charge separation and enhancement of the H_2 evolution activity. On the other hand, the presence of PS-PEG-COOH hinders charge transfer from the PITIC-ThF Pdots to the Pt cocatalyst, and AA accelerates charge recombination with less efficient photocatalytic activity of the Pdot photocatalyst. Consequently, our Pdot preparation method without a surfactant is more efficient for achieving high photocatalytic activity for H_2 evolution.

Conclusions

In summary, the different π-linkers (X = Ph, Th, ThF) are used as comonomers for the PITIC and PBTIC-based polymer preparation and they are successful in varying the absorption spectrum as well as the charge separation during the photocatalytic reaction. With a fundamental understanding of the structure–activity relationships, by fs-TAS and DFT calculation we demonstrated that the different π-linkers exhibited a significant effect on the molecular planarity accompanied by different charge transfer ability between the acceptors of different repeated moieties of the polymer. Driven by this finding, the optical properties and charge separation between D and A during photocatalytic reactions become tunable. As a result, this is the first study that presents a single polymer photocatalyst revealing excellent NIR activity (with > 780 nm cut filter) for H_2 evolution with record-breaking HER of 4100 μmol g^{-1} h^{-1} and record-breaking AQY of 4.7% at a wavelength of 700 nm. Furthermore, we demonstrated that our surfactant-free method for preparing the Pdot structure exhibited higher photocatalytic activity because the common surfactants hinder the charge transfer from Pdot particles to Pt cocatalyst or ascorbic acid (sacrificial reagent), as proved by the fs-TAS and electrochemical analysis.

Methods

Preparation of PITIC-X and PBTIC-X Pdots

Typically, a certain volume (μL) of the polymer solution (1 mg mL^{-1} in THF) was rapidly poured into water (10 mL) under sonication. Then the solution was purged with N_2 (slow rate) on a hot plate at 100°C for 90 min to remove the THF (**Figure S11**). To prepare the Pdot structure using surfactants PS-PEG-COOH or Triton, we follow the same method by adding 20% of surfactant with the polymer in the THF solution before being poured to water.

Photocatalytic H_2 evolution measurement

For measuring the H_2 evolution under visible light, the Pdot solution (0.1 mg/10 mL) containing Ascorbic Acid (AA (0.1 M)) and 3% H_2PtCl_6 cocatalyst was inserted into the reaction glass container and sealed tightly with a septum. The resulting mixture was degassed by Ar bubbling, prior to illumination. A white

light-emitting diode (LED) PAR38 lamp (20 W, 6500 K, Zenaro Lighting; λ > 420 nm) was used as the light source. While, for H_2 evolution measurement under NIR light, the Pdot solution (5 mg/10 mL) containing Ascorbic Acid (AA (0.1 M)) and 3% H_2PtCl_6 cocatalyst illuminated with light source of a Xenon lamp (AM1.5, λ > 780 nm, 3000 W m^{-2}). Hydrogen samples were taken with a gas-tight syringe and injected in a Shimazhu GC-2014 gas chromatograph, with Ar as the carrier gas. Hydrogen was detected with a thermal conductivity detector, referring to the standard hydrogen gases with known concentrations. Increased pressure from the evolved hydrogen is neglected in the calculations.

The apparent quantum yields measurement. The apparent quantum yields (AQYs) were obtained according to the following equation;

$$AQY\ (\%) = \frac{2\ \times\ Number\ of\ evolved\ H_2 molecules}{Number\ of\ incident\ photons} \times 100\%$$

$$= \frac{2 \times M \times N_A}{S \times P \times t \times {}^{\lambda}/_{(h \times c)}} \times 100\%$$

Where, M is the amount of hydrogen evolution; N_A is Avogadro constant; h is Planck constant; c is light velocity ; S is the irradiation area(5 cm^2 in our experiment); P is the incident light intensity (at 420, 500, 550, 600 and 700 nm are 20, 40, 50, 70, and 100 W m^{-2}, respectively in our experiment); t is the time of light irradiation; λ is the wavelength of monochromatic light, (420, 500, 550, 600 and 700 nm in our experiment). For the AQYs measurement, the mixed solutions were consisted of Pdot photocatalyst (5 mg/10mL water), ascorbic acid (AA, 0.1M), and 3 wt% H_2PtCl_6, it was illuminated with light source of a Xenon lamp (AM1.5).

Characterizations

^1H and ^{13}C NMR spectra were measured using a Bruker Avance 500 MHz NMR spectrometer. TGA of the polymers was performed under N_2 using a TA Q600 instrument over the temperature range 40– 550°C (heating rate: 20°C min^{-1}). UV–Vis absorption spectra of the polymers were recorded using Hitachi U-3300 and Dynamica HALO DB-20S spectrophotometers. Fluorescence spectra of the polymers were recorded using a Hitachi F-7000 spectrophotometer at room temperature. The energy levels of the HOMOs were measured using a photoelectron spectrometer (model AC-2). The optical bandgap (Eg) is derived by Tauc Plots of $(\alpha hv)^2$ versus (hv) from the UV-Vis spectra. The energy levels of the LUMOs were calculated by subtracting the Eg from the HOMO energy levels. X-ray photoelectron spectroscopy (XPS) spectra were collected using a ULVAC-PHI PHI 5000 Versaprobe II chemical analysis electron

spectrometer (ESCA). The polymers thin films were prepared from drop-casting on silicon wafer substrates for XPS measurement. The molecular geometries of the polymers were optimized, and their orbital energies and charge distributions were computed using DFT at the B3LYP/6-31G* (H, C, N, O, F, S) levels.

Transient Absorption Spectroscopy Measurement

Time-resolved experiments were performed using laser-based spectroscopy, with a laser power of less than one photon absorption per particle. Samples for transient absorption experiments were kept in the dark between measurements. A Coherent Legend Ti: Sapphire amplifier (800 nm, 100 fs pulse length, 3 kHz repetition rate) was used. The output was split to pump and probe beams. Excitation pulses at specific wavelengths were acquired using an optical parametric amplifier (Topas C, Light Conversion). The probe pulses (a broad supercontinuum spectrum) were generated from the 800-nm pulses in a CaF_2 crystal and split by a beam splitter into a probe pulse and a reference pulse. The probe pulse and the reference pulse were dispersed in a spectrograph and detected by a diode array. The instrumental response time was approximately 100 fs. The kinetic traces were fitted with a sum of convoluted exponentials:

$$\mathrm{Y}(t) = \mathrm{ext}\left[-\frac{(\mathrm{t}-\mathrm{t_0})^2}{\tau_\mathrm{p}}\right] * \sum_\mathrm{i} \mathrm{A_i}\, \exp\left(-\frac{\mathrm{t}-\mathrm{t_0}}{\tau_\mathrm{i}}\right)$$

where $\tau_\mathrm{p} = \frac{\mathrm{IRF}}{2\ln 2}$ and IRF is the width of the instrument response function (full width at half-maximum), $\mathrm{t_0}$ is the time zero, $\mathrm{A_i}$ and τ_i are amplitude and decay times, respectively, and * is the convolution operator.

Cryo-tem And Cry-ed

The nano-polymer morphologies were examined by a FEI Tecnai G2 F20 bioTWIN Transmission Electron Microscope at 200 keV. Four µL of the sample containing ~ 1 mg/ml nanoparticles were pipetted onto a glow-discharged (15 seconds on the carbon side) 200-mesh copper grids (HC200-Cu, PELCO), which were blotted in a chamber at 100% humidity at 4°C for 3 seconds and plunge-frozen into liquid ethane cooled by liquid nitrogen using a Vitrobot (FEI, Hillsboro, OR). The grid was stored in liquid nitrogen until mounted for imaging. Cryo-transmission electron microscopy images were recorded at a defocus of ~ 1-1.2 µm under low-dose exposures (2800 e/nm^2.s) with a 4kx4k charge-coupled device camera (Glatan, Pleasanton, CA) at a magnification of 80,000X. Images and electron diffraction patterns were recorded in the low-dose mode to minimize electron beam radiation damage to the very radiation-sensitive samples.

Declarations

Associated Content

Supporting Information

Supporting Information related to this article can be found in the online version, at doi:—— .

Author Information

*Corresponding Author E-mail: hhchou@mx.nthu.edu.tw

Note

The author declares no conflict of interest.

Acknowledgements

The authors gratefully acknowledge the financial support of National Science and Technology Council of Taiwan (NSTC 111-2628-E-007-009- and 110-2123-M-002-006), Science Vanguard Project of National Science and Technology Council (NSTC) [110-2123-M-002-006]; the iMATE program of Academia Sinica [AS-iMATE-110-34]; and the Center of Atomic Initiative for New Materials (AI-Mat), National Taiwan University, from the Featured Areas Research Center Program within the framework of the Higher Education Sprout Project by the Ministry of Education (MOE) of Taiwan [110 L9008]. The authors appreciate the Precision Instrument Support Center of National Tsing Hua University in providing the analysis and measurement facilities. The authors appreciate for Dr. Yuan-Chih Chang for cryo-EM experiments which performed at the Academia Sinica Cryo-EM Facility (ASCEM).

References

1. Dai CH, Liu B. Conjugated polymers for visible-light-driven photocatalysis. Energy Environ. Sci. **13**, 24–52 (2020).
2. Banerjee T, Podjaski F, Kröger J, Biswal BP, Lotsch BV. Polymer photocatalysts for solar-to-chemical energy conversion. Nat. Rev. Mater. **6**, 168–190 (2021).
3. Wang Y, *et al.* Current understanding and challenges of solar-driven hydrogen generation using polymeric photocatalysts. Nat. Energy **4**, 746–760 (2019).
4. Wang X, *et al.* Sulfone-containing covalent organic frameworks for photocatalytic hydrogen evolution from water. Nat. Chem. **10**, 1180–1189 (2018).
5. Shu C, *et al.* Boosting the Photocatalytic Hydrogen Evolution Activity for D–π–A Conjugated Microporous Polymers by Statistical Copolymerization. Adv. Mater. **33**, 2008498 (2021).
6. Pati PB, *et al.* An experimental and theoretical study of an efficient polymer nano-photocatalyst for hydrogen evolution. Energy Environ. Sci. **10**, 1372–1376 (2017).
7. Liu A, *et al.* Panchromatic Ternary Polymer Dots Involving Sub-Picosecond Energy and Charge Transfer for Efficient and Stable Photocatalytic Hydrogen Evolution. J. Am. Chem. Soc. **143**, 2875–

2885 (2021).

8. Elsayed MH, *et al.* Visible-light-driven hydrogen evolution using nitrogen-doped carbon quantum dot-implanted polymer dots as metal-free photocatalysts. Appl. Catal. B-Environ. **283**, 119659 (2021).
9. Kosco J, *et al.* Generation of long-lived charges in organic semiconductor heterojunction nanoparticles for efficient photocatalytic hydrogen evolution. Nat. Energy **7**, 340–351 (2022).
10. Kosco J, *et al.* Enhanced photocatalytic hydrogen evolution from organic semiconductor heterojunction nanoparticles. Nat. Mater. **19**, 559–565 (2020).
11. An S, Hassan SZ, Jung J-W, Cha H, Cho C-H, Chung DS. Covalent Networking of a Conjugated-Polymer Photocatalyst to Promote Exciton Diffusion in the Aqueous Phase for Efficient Hydrogen Production. Small Methods **6**, 2200010 (2022).
12. Elsayed MH, *et al.* Hydrophobic and Hydrophilic Conjugated Polymer Dots as Binary Photocatalysts for Enhanced Visible-Light-Driven Hydrogen Evolution through Förster Resonance Energy Transfer. ACS Appl. Mater. Interfaces **13**, 56554–56565 (2021).
13. Lin W-C, *et al.* Sulfide oxidation tuning in 4,8-bis(5-(2-ethylhexyl)thiophen-2-yl)benzo[1,2-b:4,5-b']dithiophene based dual acceptor copolymers for highly efficient photocatalytic hydrogen evolution. J. Mater. Chem. A **10**, 6641–6648 (2022).
14. Lin W-C, *et al.* Effect of energy bandgap and sacrificial agents of cyclopentadithiophene-based polymers for enhanced photocatalytic hydrogen evolution. Appl. Catal. B-Environ. **298**, 120577 (2021).
15. Elewa AM, El-Mahdy AFM, Elsayed MH, Mohamed MG, Kuo S-W, Chou H-H. Sulfur-doped triazine-conjugated microporous polymers for achieving the robust visible-light-driven hydrogen evolution. Chem. Eng. J. **421**, 129825 (2021).
16. Bai Y, Wilbraham L, Slater BJ, Zwijnenburg MA, Sprick RS, Cooper AI. Accelerated Discovery of Organic Polymer Photocatalysts for Hydrogen Evolution from Water through the Integration of Experiment and Theory. J. Am. Chem. Soc. **141**, 9063–9071 (2019).
17. Sprick RS, *et al.* Tunable Organic Photocatalysts for Visible-Light-Driven Hydrogen Evolution. J. Am. Chem. Soc. **137**, 3265–3270 (2015).
18. Sachs M, *et al.* Understanding structure-activity relationships in linear polymer photocatalysts for hydrogen evolution. Nat. Commun. **9**, 4968 (2018).
19. Woods DJ, *et al.* Side-chain tuning in conjugated polymer photocatalysts for improved hydrogen production from water. Energy Environ. Sci. **13**, 1843–1855 (2020).
20. Cai X, *et al.* Au Nanorod Photosensitized La2Ti2O7 Nanosteps: Successive Surface Heterojunctions Boosting Visible to Near-Infrared Photocatalytic H2 Evolution. ACS Catal. **8**, 122–131 (2017).
21. Zhu M, *et al.* Metal-Free Photocatalyst for H2 Evolution in Visible to Near-Infrared Region: Black Phosphorus/Graphitic Carbon Nitride. J. Am. Chem. Soc. **139**, 13234–13242 (2017).
22. Cai X, *et al.* Au Nanorod Photosensitized La2Ti2O7 Nanosteps: Successive Surface Heterojunctions Boosting Visible to Near-Infrared Photocatalytic H_2 Evolution. ACS Catal. **8**, 122–131 (2018).

23. Elbanna O, Zhu M, Fujitsuka M, Majima T. Black Phosphorus Sensitized TiO2 Mesocrystal Photocatalyst for Hydrogen Evolution with Visible and Near-Infrared Light Irradiation. ACS Catal. **9**, 3618–3626 (2019).
24. Xu Y, *et al.* Homogeneous Carbon/Potassium-Incorporation Strategy for Synthesizing Red Polymeric Carbon Nitride Capable of Near-Infrared Photocatalytic H2 Production. Adv. Mater. **33**, 2101455 (2021).
25. Liu Y, *et al.* Ultrastable metal-free near-infrared-driven photocatalysts for H2 production based on protonated 2D g-C3N4 sensitized with Chlorin e6. Appl. Catal. B-Environ. **260**, 118137 (2020).
26. Lin Y, *et al.* An Electron Acceptor Challenging Fullerenes for Efficient Polymer Solar Cells. Adv. Mater. **27**, 1170–1174 (2015).
27. Yuan J, *et al.* Fused Benzothiadiazole: A Building Block for n-Type Organic Acceptor to Achieve High-Performance Organic Solar Cells. Adv. Mater. **31**, 1807577 (2019).
28. Cheng P, Li G, Zhan X, Yang Y. Next-generation organic photovoltaics based on non-fullerene acceptors. Nat. Photonics **12**, 131–142 (2018).
29. Hou J, Inganäs O, Friend RH, Gao F. Organic solar cells based on non-fullerene acceptors. Nat. Mater. **17**, 119–128 (2018).
30. Yan C, *et al.* Non-fullerene acceptors for organic solar cells. Nat. Rev. Mater. **3**, 18003 (2018).
31. Zhu L, *et al.* Single-junction organic solar cells with over 19% efficiency enabled by a refined double-fibril network morphology. Nat. Mater. **21**, 656–663 (2022).
32. Yuan J, *et al.* Single-Junction Organic Solar Cell with over 15% Efficiency Using Fused-Ring Acceptor with Electron-Deficient Core. Joule **3**, 1140–1151 (2019).
33. Yang H, Li X, Sprick RS, Cooper AI. Conjugated polymer donor–molecular acceptor nanohybrids for photocatalytic hydrogen evolution. Chem. Commun. **56**, 6790–6793 (2020).
34. Elsayed MH, *et al.* Indacenodithiophene-based N-type conjugated polymers provide highly thermally stable ternary organic photovoltaics displaying a performance of 17.5%. J. Mater. Chem. A, (2021).
35. Lin W-C, *et al.* Design and synthesis of cyclometalated iridium-based polymer dots as photocatalysts for visible light-driven hydrogen evolution. Int. J. Hydrog. Energy **45**, 32072–32081 (2020).
36. Wang L, *et al.* Organic Polymer Dots as Photocatalysts for Visible Light-Driven Hydrogen Generation. Angew. Chem.-Int. Edit. **55**, 12306–12310 (2016).
37. Tseng P-J, *et al.* Design and Synthesis of Cycloplatinated Polymer Dots as Photocatalysts for Visible-Light-Driven Hydrogen Evolution. ACS Catal. **8**, 7766–7772 (2018).
38. Elsayed MH, *et al.* Hydrophobic and Hydrophilic Conjugated Polymer Dots as Binary Photocatalysts for Enhanced Visible-Light-Driven Hydrogen Evolution through Forster Resonance Energy Transfer. ACS Appl. Mater. Interfaces, **13**, 56554–56565 (2021).
39. Biswal HS, Shirhatti PR, Wategaonkar S. O – H··· O versus O – H··· S hydrogen bonding I: experimental and computational studies on the p-cresol· H_2O and p-cresol· H_2S complexes. J. Phys. Chem. A **113**, 5633–5643 (2009).

40. Ghosh S, Chopra P, Wategaonkar S. C–H··· S interaction exhibits all the characteristics of conventional hydrogen bonds. Phys. Chem. Chem. Phys. **22**, 17482–17493 (2020).
41. Zheng YQ, *et al.* Strong Electron-Deficient Polymers Lead to High Electron Mobility in Air and Their Morphology-Dependent Transport Behaviors. Adv. Mater. **28**, 7213–7219 (2016).
42. Woods DJ, *et al.* Side-chain tuning in conjugated polymer photocatalysts for improved hydrogen production from water. Energy Environ. Sci. **13**, 1843–1855 (2020).

Figures

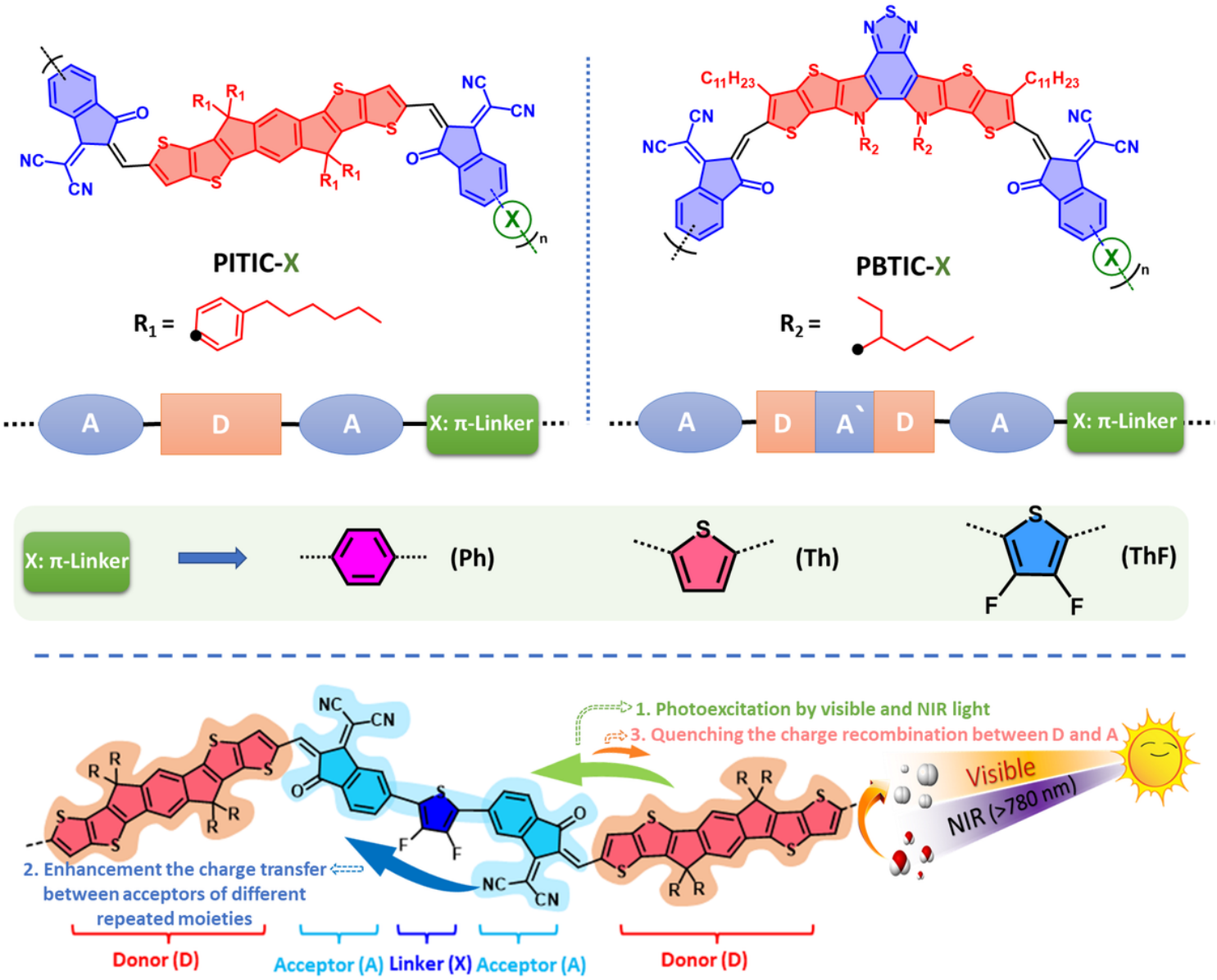

Figure 1

Chemical structures of the PITIC-X and PBTIC-X polymers featuring various π-linker units (X = Ph, Th, and ThF). In addition, schematic diagram showing the charge transfer through the PITIC-ThF polymer chain

during the photocatalytic reaction under visible and NIR light.

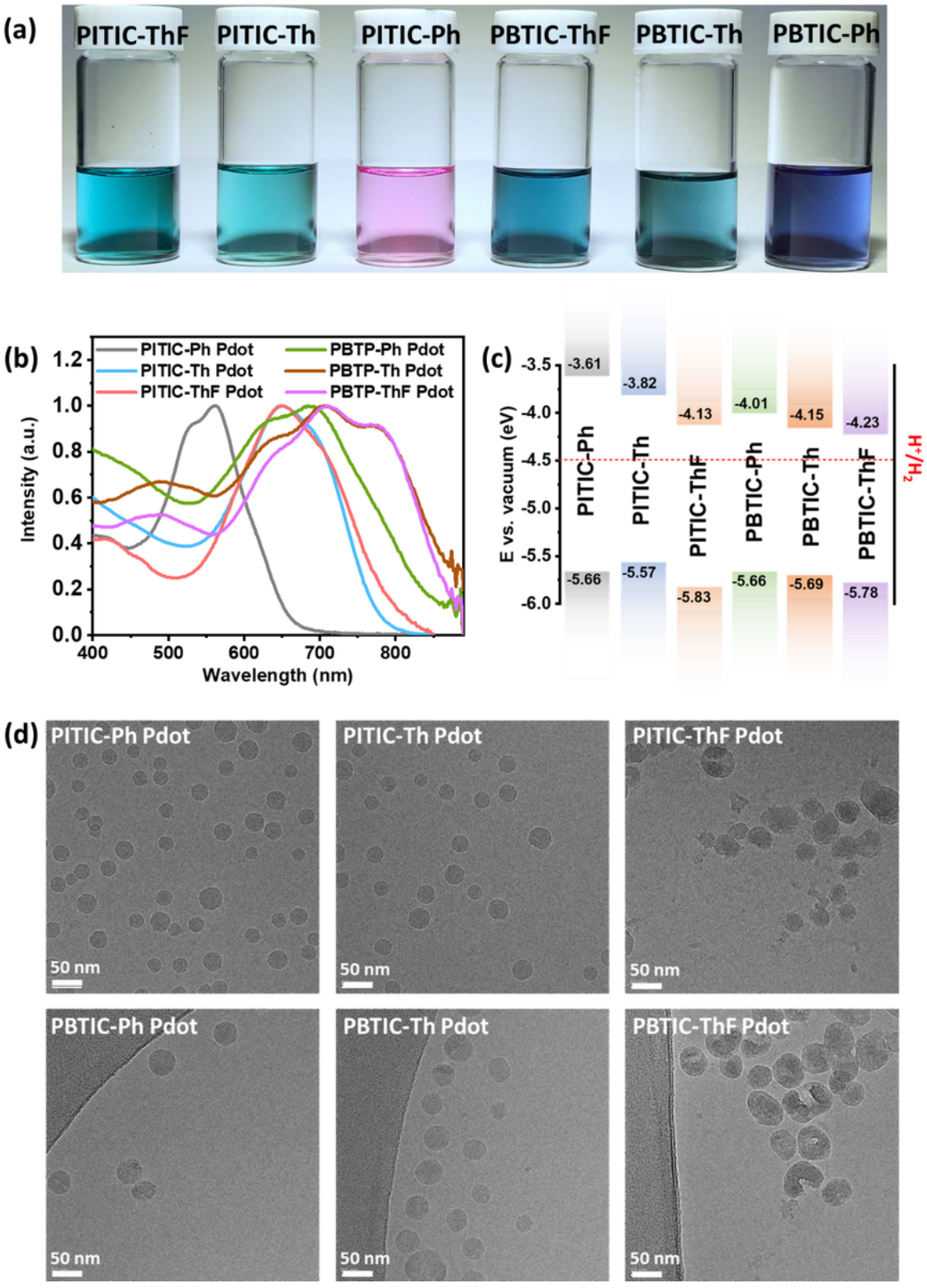

Figure 2

(a) Photographs of the six polymers in THF solutions, (b) UV–Vis absorption spectra of the all-polymer dots in water solutions and (c) energy level diagrams of the all-polymers, (d) Cryo-TEM of PITIC-Ph Pdots, PITIC-Th Pdots, PITIC-ThF Pdots, PBTIC-Ph Pdots, PBTIC-Th Pdots, and PBTIC-ThF Pdots.

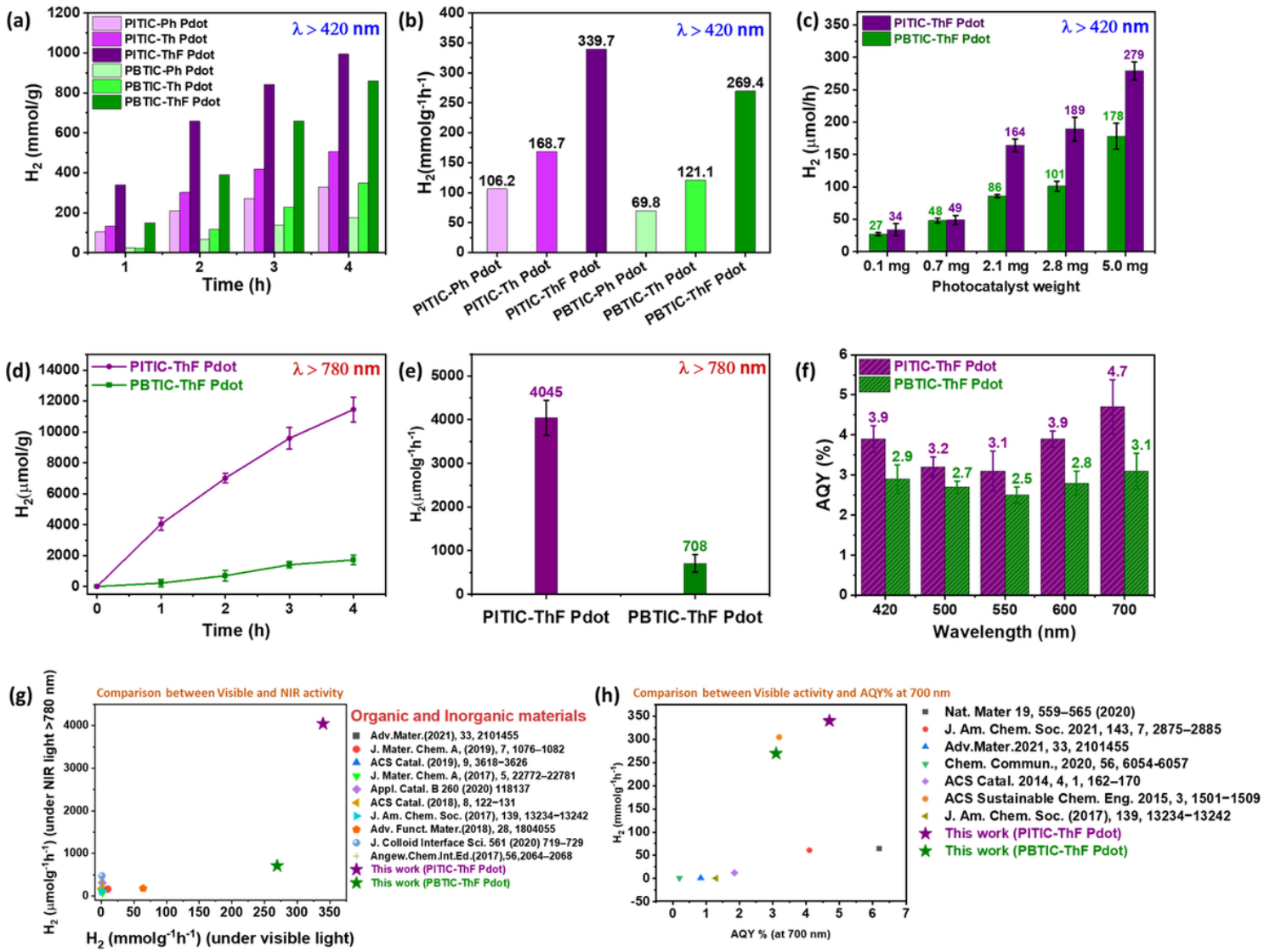

Figure 3

a) Time course of the produced H_2 of the six Pdots. b) HER of the six Pdots. c) HER of the PITIC-ThF Pdots and PBTIC-ThF Pdots with different photocatalyst weights. Conditions: ascorbic acid (AA, 0.1 M), white LED light (λ > 420 nm, 20 W, and 6500 K), and 3% H_2PtCl_6. d) Time course of the produced H_2 for the PITIC-ThF and PBTIC-ThF Pdots under NIR light. e) HER of PITIC-ThF and PBTIC-ThF Pdots under NIR light. Conditions: ascorbic acid (AA, 0.1 M), 3% H_2PtCl_6, and a xenon lamp light source (λ >780 nm, and 3000 W m^{-2}). f) Apparent quantum yields for the PITIC-ThF Pdots and PBTIC-ThF Pdots at different wavelengths. g) Comparison of HER under visible and NIR light and h) comparison of HER with AQY% of PITIC-ThF Pdot and PBTIC-ThF Pdot with the literature-reported photocatalysts.

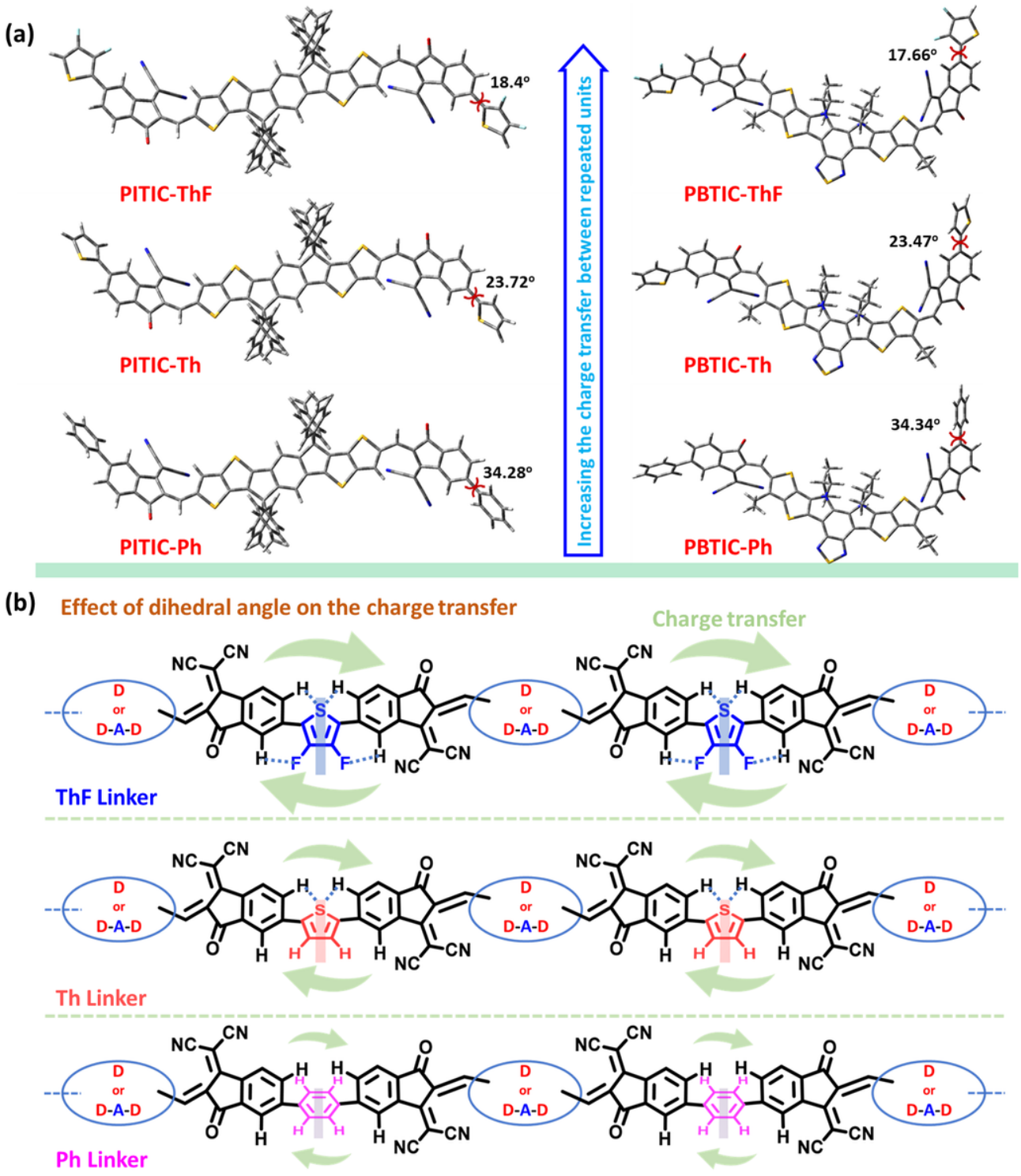

Figure 4

(a) DFT geometry optimization of the polymers with the calculated dihedral angle. (b) Schematic diagram showing the dihedral angle effect of different π-linkers on the charge transfer between acceptors of repeated moieties.

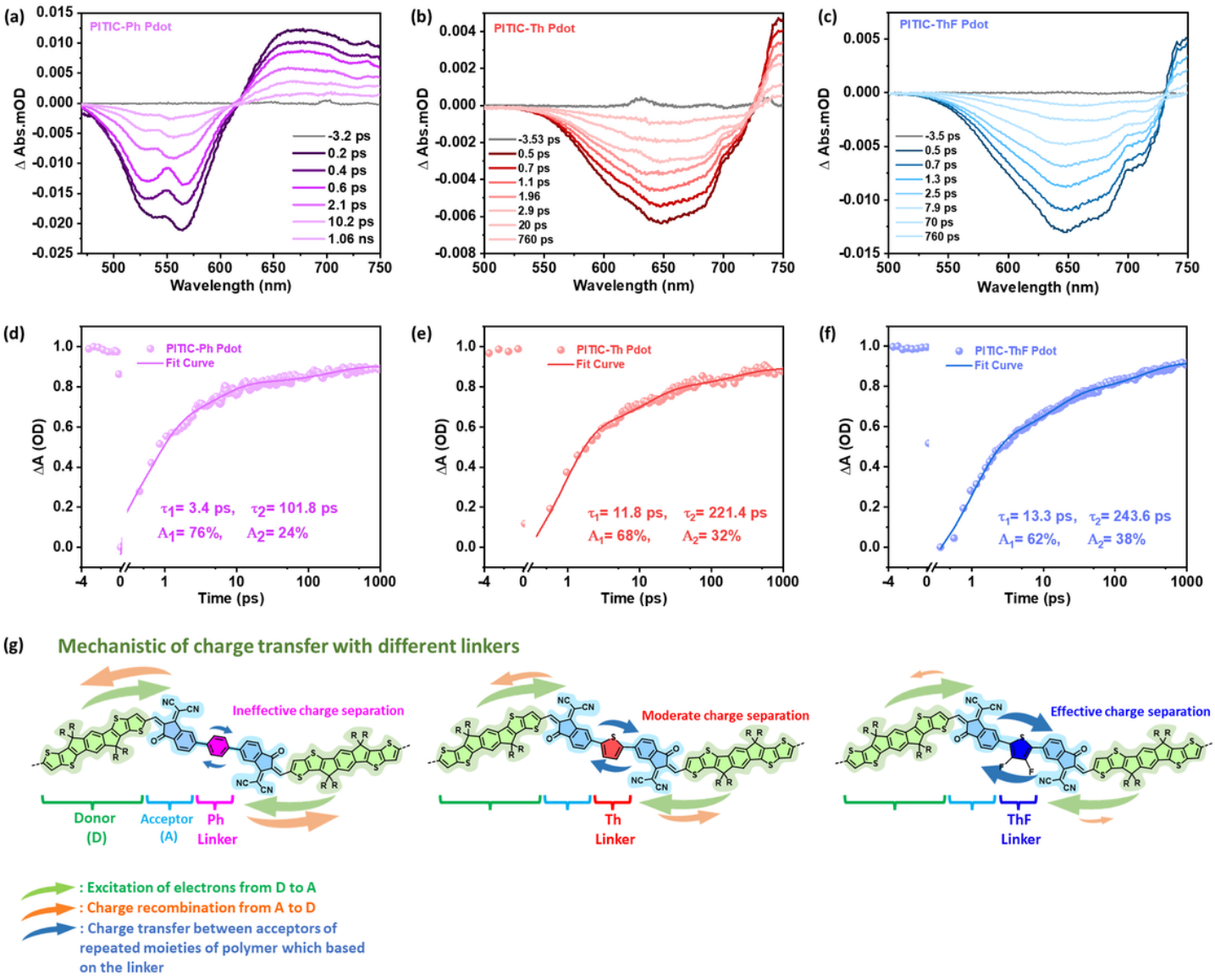

Figure 5

Transient absorption spectra of (a) PITIC-Ph Pdots (water solution), (b) PITIC-Th Pdots, and (c) PITIC-ThF Pdots at different delay times. Transient absorption traces of (d) PITIC-Ph Pdot, (e) PITIC-Th Pdots, and (f) PITIC-ThF Pdots. The data were obtained using an excitation wavelength of 550 nm and a power of 10 μW. (g) Schematic diagram presenting the effect of different likers on the charge transfer between acceptors of repeated moieties of the polymer and the charge recombination between the acceptor and donor.

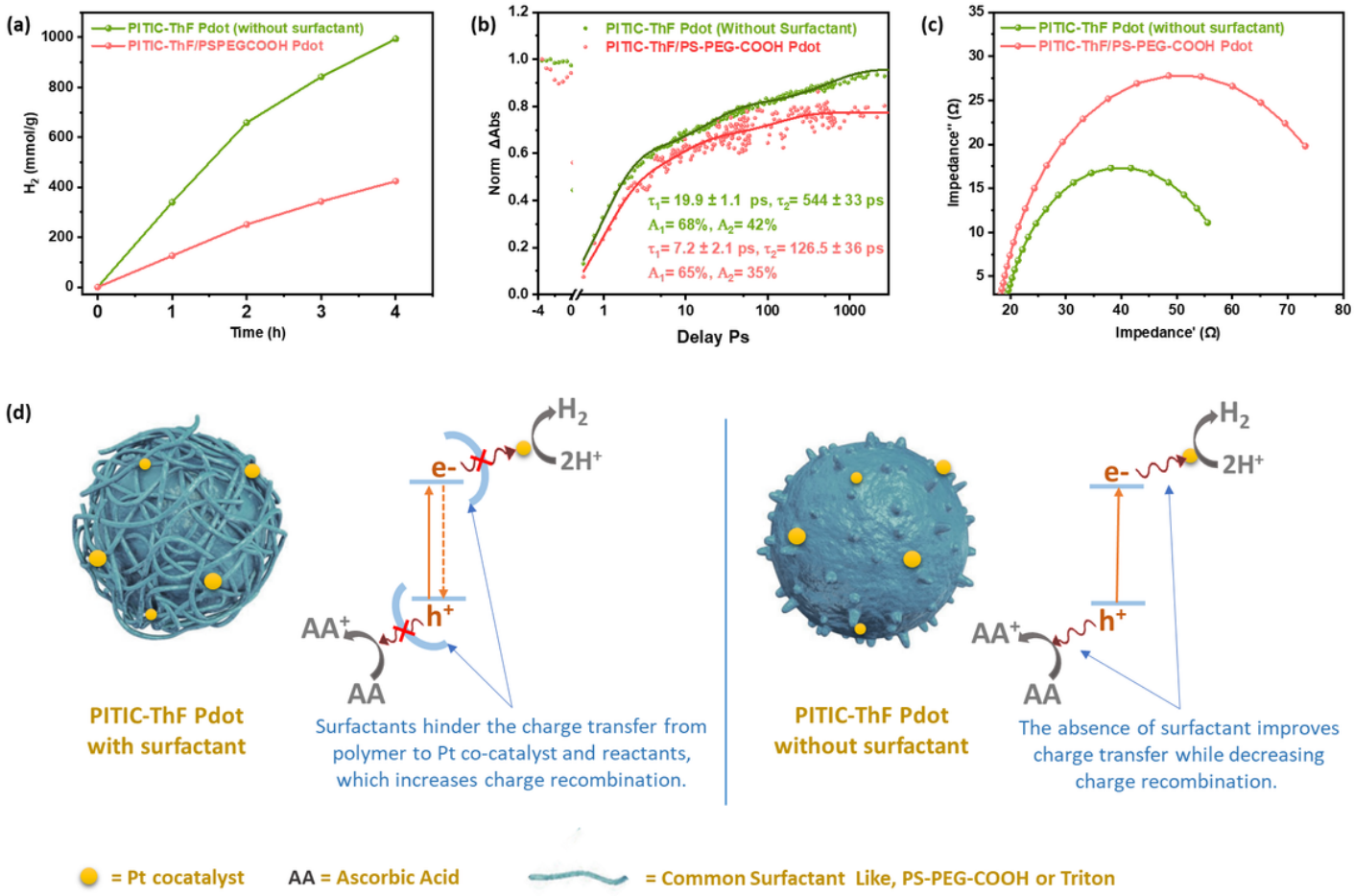

Figure 6

(a) Effect of PS-PEGCOOH surfactant on the photocatalytic hydrogen production activity of the PITIC-ThF Pdots. (b) Transient absorption traces of PITIC-ThF Pdot in the presence of Pt co-catalyst (with and without a surfactant). The data were obtained using an excitation wavelength of 550 nm and a power of 10 μW. (c) Electrochemical impedance spectroscopy (EIS) of the PITIC-ThF Pdots (with and without a surfactant). (d) Schematic diagram of the PITIC-ThF Pdots (with and without a surfactant) presenting the effect of the surfactant on the charge transfer between the Pdots and Pt cocatalyst.

Supplementary Files

This is a list of supplementary files associated with this preprint. Click to download.

- SupportingInformationNatComm202212.docx